Exploration of BioMat-X

Open Exploration

Open Access Original Article

Biogenic carbon quantum dots with tunable surface charge for biocompatible antibacterial applications

Hong Yin[1,2*], Manjul Gautam[3], Xingjian Gong[3,4], Tahlia J. Stewart[4], Paul N. Smith[4,5,6], Ivan Cole[1,2], Rachel W. Li[3,4,6]

[1]School of Engineering, The Australian National University, Canberra ACT 2601, Australia
[2]School of Engineering, STEM College, RMIT University, Melbourne VIC 3000, Australia
[3]John Curtin School of Medical Research, The Australian National University, Canberra ACT 2601, Australia
[4]The Canberra Hospital, Garran ACT 2605, Australia
[5]Orthopaedics ACT, Woden Specialist Medical Centre, Phillip ACT 2606, Australia
[6]School of Medicine and Psychology, The Australian National University, Canberra ACT 2601, Australia

***Correspondence:** Hong Yin, School of Engineering, The Australian National University, Canberra, ACT 2601, Australia. hong.yin@anu.edu.au
Academic Editor: Arthur Ragauskas, The University of Tennessee, USA
Received: April 27, 2026 **Accepted:** August 26, 2026 **Published:** September 9, 2026

Cite this article: Yin H, Gautam M, Gong X, Stewart TJ, Smith PN, Cole I, et al. Biogenic carbon quantum dots with tunable surface charge for biocompatible antibacterial applications. Explor BioMat-X. 2026;3:101373. https://doi.org/10.37349/ebmx.2026.101373

Abstract

Aim: Antimicrobial resistance poses a major global health crisis, with some bacterial strains now resistant to nearly all available antibiotics. Carbon quantum dots (CQDs) have emerged as promising nanomaterials for broad-spectrum infection prevention owing to their multiple antibacterial mechanisms, biocompatibility, and cost-effectiveness. Many reported CQD fabrication methods rely on synthetic chemicals, which increase production costs and potentially compromise the biocompatibility of the resulting CQDs. Although green-synthesized CQDs have attracted considerable attention for antibacterial applications, limited studies have investigated the use of natural, food-derived components to tune CQD surface charge and its influence on antibacterial activity and mammalian cell compatibility. This study aims to develop CQDs with tunable surface charges from natural food-derived carbon sources for broad-spectrum antibacterial applications.

Methods: Whole-meal bread and soybean flour were used as biogenic precursors to synthesize negatively charged CQDs via a simple hydrothermal method. Surface charge was adjusted to neutral and positive by incorporating lemon juice and chitosan during synthesis. Antibacterial activity and mammalian cell viability were evaluated.

Results: Bread- and soybean-derived CQDs exhibited negative surface charges (–15 mV) due to abundant carboxyl and hydroxyl groups formed during precursor decomposition. Addition of lemon juice altered the surface chemistry by introducing balanced protonated and deprotonated species, producing zwitterionic CQDs with near-neutral charge (–0.1 mV). Further incorporation of chitosan introduced protonated amine groups ($-NH_3^+$), yielding positively charged CQDs (+10 mV). At an optimal concentration of 10 μg/mL, both neutral and positively charged CQDs demonstrated moderate broad-spectrum antibacterial activity

(30–40% inhibition) against Gram-negative and Gram-positive bacteria. Their antibacterial effect was attributed to favorable electrostatic interactions with negatively charged bacterial cell envelopes, causing membrane disruption, reactive oxygen species (ROS)-induced damage, and intracellular interference. In contrast, mammalian cells maintained 100% viability, likely due to their flexible cholesterol-rich membranes, stronger antioxidant defense systems, and intracellular compartmentalization.

Conclusions: This study demonstrates a reagent-free and sustainable approach for producing CQDs with controlled surface charges from natural precursors. The resulting CQDs show strong potential as safe and effective antibacterial nanomaterials for biomedical applications.

Keywords

carbon quantum dots, surface charge, biogenic precursors, antibacterial activity, biocompatibility

Introduction

Carbon quantum dots (CQDs), a rapidly developing class of carbon-based nanomaterials, have attracted significant research attention over the past decade owing to their simple synthesis methods, excellent biocompatibility, low toxicity, and high photostability [1]. They have found extensive applications in various fields, including bioimaging, drug delivery, sensing, photocatalysis, and optoelectronic technologies. Recently, CQDs have been reported as promising antibacterial agents [2]. Unlike conventional antibiotics, the antibacterial activity of CQDs is achieved through multiple pathways, including membrane disruption, biofilm inhibition, reactive oxygen species (ROS) generation, intracellular interactions, and photoinduced effects such as photodynamic therapy (PDT) and photothermal therapy (PTT). These mechanisms often act synergistically to enhance the overall antibacterial performance and reduce the likelihood of antimicrobial resistance [3–15]. Positively charged CQDs generally possess strong antimicrobial activity because of their strong electrostatic interactions with negatively charged bacterial membranes, leading to membrane disruption and bacterial cell death [16]. Some researchers raised an issue that the synthesis of these CQDs often involves toxic precursors, which pose environmental risks and limit their practical applications [17].

The demand for biocompatible and cost-effective CQDs has driven their synthesis from biogenic sources [18]. Researchers have reported that various vegetables, fruits, and plant-derived materials, including orange juice [19], carrot [20], cherry tomato [21], lemon peel [22], onion waste [23], taro peel [24], watermelon peel [25], and banana peel [26], have been utilized as carbon precursors. The current issue is that many fabrication processes still rely on synthetic chemicals, which compromise the inherent biocompatibility of CQDs [27, 28]. Recently, Gokul Eswaran et al. [29] successfully synthesized highly fluorescent CQDs from bread waste without using any additional reagents; however, their hydrothermal process demanded high energy input and prolonged reaction time (13 h). In our previous work, we demonstrated the fabrication of biocompatible CQDs from bread using a chemical-free method [30]. However, the surface charge of these CQDs is mainly negative, and positively charged CQDs prepared from biogenic precursors have not been widely reported. Surface charge is particularly important because it can influence the interaction of CQDs with bacterial cell envelopes and, consequently, their antibacterial activity [31]. However, systematic studies on surface-charge-controlled CQDs derived from biogenic precursors remain limited, and developing such CQDs could help clarify the effects of surface charge on their antibacterial activities.

In this study, we used whole meal bread and soybean flour as biogenic precursors to synthesize CQDs with negative charges via a simple hydrothermal method. The surface charge of the CQDs was tuned by incorporating lemon juice and chitosan during synthesis. Chitosan is a natural, biodegradable polymer derived from chitin, which is a major component of the shells of crustaceans such as shrimp, crabs, and lobsters. This work successfully demonstrates the controlled preparation of CQDs with distinct surface charges using biogenic and environmentally benign precursors and systematically evaluates the effect of surface charge on their antibacterial properties.

Materials and methods

Preparation of CQDs

Negatively charged CQDs were prepared by a previously reported method [30, 32]. Briefly, whole-meal bread (1 g) and soybean flour (4 g) purchased from the local supermarket were mixed in 30 mL of deionized water. The mixture was sonicated for 5 min and subjected to a hydrothermal reaction at 180ºC for 4 h. After cooling overnight, the product was centrifuged at 3,000 rpm for 5 min, and the collected supernatant was filtered using a number 1 (90 mm) filter paper and a 0.22 μm syringe filter. The sample was freeze-dried and stored at 4°C. For the preparation of neutrally charged CQDs, the 30 mL of deionized water was replaced with freshly squeezed pulp-free lemon juice. The rest of the procedures, including sonication, heating, centrifugation, and filtration, were the same as in the preparation of negatively charged CQDs. For the preparation of positively charged CQDs, after mixing whole-meal bread, soybean flour, and lemon juice and sonicating for 5 min, 2 g of chitosan was added to the mixture and completely dissolved. The remaining procedures were the same as above.

Characterizations

Transmission electron microscopy (TEM) was performed with a JEOL 1010 TEM 868 (JEOL, Sydney, Australia) operated at 100 kV. Before imaging, the CQD suspension was sonicated for 20 min. The supernatant was then drop-cast onto a carbon-coated grid and dried overnight under ambient conditions. Fourier-transform infrared spectroscopy (FTIR) was used to characterize the chemical functionalities of the CQDs. Spectra were collected using a PerkinElmer Frontier FTIR spectrometer (Waltham, MA, USA) over 4,000–500 cm^{-1}, with a spectral resolution of 4 cm^{-1} and 32 scans averaged for each measurement. The surface chemical composition and bonding states were analyzed by X-ray photoelectron spectroscopy (XPS) using a Thermo Scientific K-Alpha system (Thermo Fisher Scientific, UK) equipped with a monochromatic Al Kα source ($h\nu$ = 1,486.7 eV). The analysis chamber was maintained at a base pressure below 1×10^{-9} mbar. CasaXPS software (version 2.3.25PR1.0) was used for data processing and peak fitting. The zeta potential of the CQDs was measured using a Malvern Zetasizer Nano Z system (ZEN2600, Malvern Instruments, UK).

Biocompatibility assays

Fibroblast cells obtained from the American Type Culture Collection (ATCC, Rockville, MD, USA) were identified via STR analysis and are free of mycoplasma contamination. Cells were cultured in Dulbecco's modified eagle medium (DMEM) supplemented with 10% heat-inactivated fetal bovine serum (FBS), 2 mM *L*-glutamine, and antibiotics at 37ºC in a humidified 5% CO_2 atmosphere. All cell cultures were maintained under strictly controlled aseptic conditions, including sterilization of equipment and media, biosafety cabinet use, and proper handling, transport, and disposal procedures, ensuring contamination-free cultures. The cells were seeded in a 24-well plate and allowed to adhere for 2 h. Then, CQDs of various concentrations (1, 10, and 100 μg/mL) were introduced to the cells, followed by incubation at 37°C, 5% CO_2 for a week. The media was replaced twice during the week. At the end of culture, the supernatant was aspirated, and the attached cells were rinsed with phosphate-buffered saline (PBS) twice. Cell viability was detected using the ATPlite luminescence assay kit (Part #6016943, PerkinElmer, Australia). Briefly, after adding 50 μL of mammalian cell lysis solution to each well and shaking the plate for 2 min in an orbital shaker at 700 rpm, 50 μL of the luciferase/luciferin solution was added to each well. The plate was read in a dark chamber of an Infinite M200 PRO plate reader (Tecan, Australia) to measure luminescence. The percentage (%) of increment or decrement in cell viability was calculated through normalization to the control (media only).

Antibacterial activities

Periprosthetic joint infection (PJI) is a severe complication following total joint arthroplasty (TJA), often requiring prolonged antibiotic treatment [14]. The most common pathogens that cause PJI include Gram-positive *Staphylococcus aureus* and *Staphylococcus epidermidis*, which are responsible for up to 60% of all

prosthetic hip implant infections. *Escherichia coli* is the most common Gram-negative bacterium related to PJI. Therefore, we tested CQDs for their antibacterial efficacy using the above three strains in this study.

Bacteria were obtained from Professor Siming Man's laboratory at John Curtin School of Medical Research (JCSMR) and Microbiology Unit, Canberra Health Services, Australia. Bacterial suspensions were seeded into a 24-well plate at a density of 1.5×10^4 CFU/mL. CQDs were dispersed in distilled water (H_2O) and added to the bacterial culture at 3 concentrations (1, 10, and 100 μg/mL). The plates were placed on a shaker at 37ºC for 24 h. The negative control was bacteria without any CQD treatment. All experimental conditions were performed in 6 replicates.

Following incubation, the cultures were stained with 3 μL of LIVE/DEAD BacLight bacterial viability kit (Cat. No. L7012, Thermo Fisher Scientific, Australia) and incubated in the dark at room temperature for 10 min. Subsequently, 200 μL of each suspension was pipetted into wells of a PerkinElmer 96-well flat black plate. Fluorescence measurements were performed using an Infinite M200 PRO plate reader with an excitation wavelength of 470 nm and an emission wavelength of 550 nm. The measured emission intensity corresponds to the number of live bacteria. Intensity readings of empty wells representing background signals were averaged and deducted from the intensity readings of the samples. The average intensity of the negative control replicates was calculated. The following equation was used to derive the inhibition of growth of all test samples based on the assumption that the media alone do not inhibit bacterial growth:

$$Inhibition\ of\ growth\ (\%) = 1 - \frac{Test\ sample\ intensity\ reading}{Negative\ control\ intensity\ reading} \times 100$$

Statistical analysis

All experimental conditions were tested in six replicates. Results are presented as mean ± standard error of the mean (SEM). Differences in cell viability between CQD-treated and untreated samples were assessed using Student's *t*-test, with $p < 0.05$ considered statistically significant.

Results

Characterization of CQDs

Figure 1a shows the precursors used in the synthesis and the measured surface charges of the CQDs. Using wholemeal bread and soy flour as carbon precursors and deionized water as the reaction medium, the resulting CQDs have a zeta potential of –15 mV, indicating that the surface is dominated by anionic groups, such as carboxyl or hydroxyl groups. If the reaction medium was replaced with lemon juice, the obtained CQDs had a zeta potential of –0.1 mV, which is characterized by the presence of equal amounts of cationic and anionic groups. When chitosan was introduced to the wholemeal bread + soy flour + lemon juice hydrothermal reaction system, a zeta potential of +10 mV was achieved, suggesting the positive charge of the CQDs.

The morphology and size of the CQDs with different surface charges were examined using TEM, and the corresponding images are presented in Figure 1b. All three CQDs exhibited similar morphology; however, the neutral CQDs showed a higher tendency to agglomerate than the negatively and positively charged ones, which can be attributed to the absence of electrostatic repulsion between particles.

Figure 1c shows the fluorescence spectra of these CQDs at an excitation wavelength of 360 nm, with a broad peak observed in the range of 400–500 nm. The CQDs with negative and positive charges had similar but low fluorescence intensity. The neutral CQDs have the highest fluorescence intensity. This observation is consistent with the findings of Radchanka et al. [33], who reported that the net charge density within the slipping plane can affect the nonradiative recombination processes of quantum dots. Generally, quantum dots bearing zwitterionic surface groups and exhibiting low surface charges are associated with high quantum yields and strong fluorescence.

The functional groups attached to the CQDs with different surface charges were characterized by FTIR spectroscopy. As shown in Figure 1d, the strong peaks around 850–1,150 cm^{-1} in the fingerprint region corresponded to the carbohydrate groups in the bread. These peaks are the strongest in the negatively

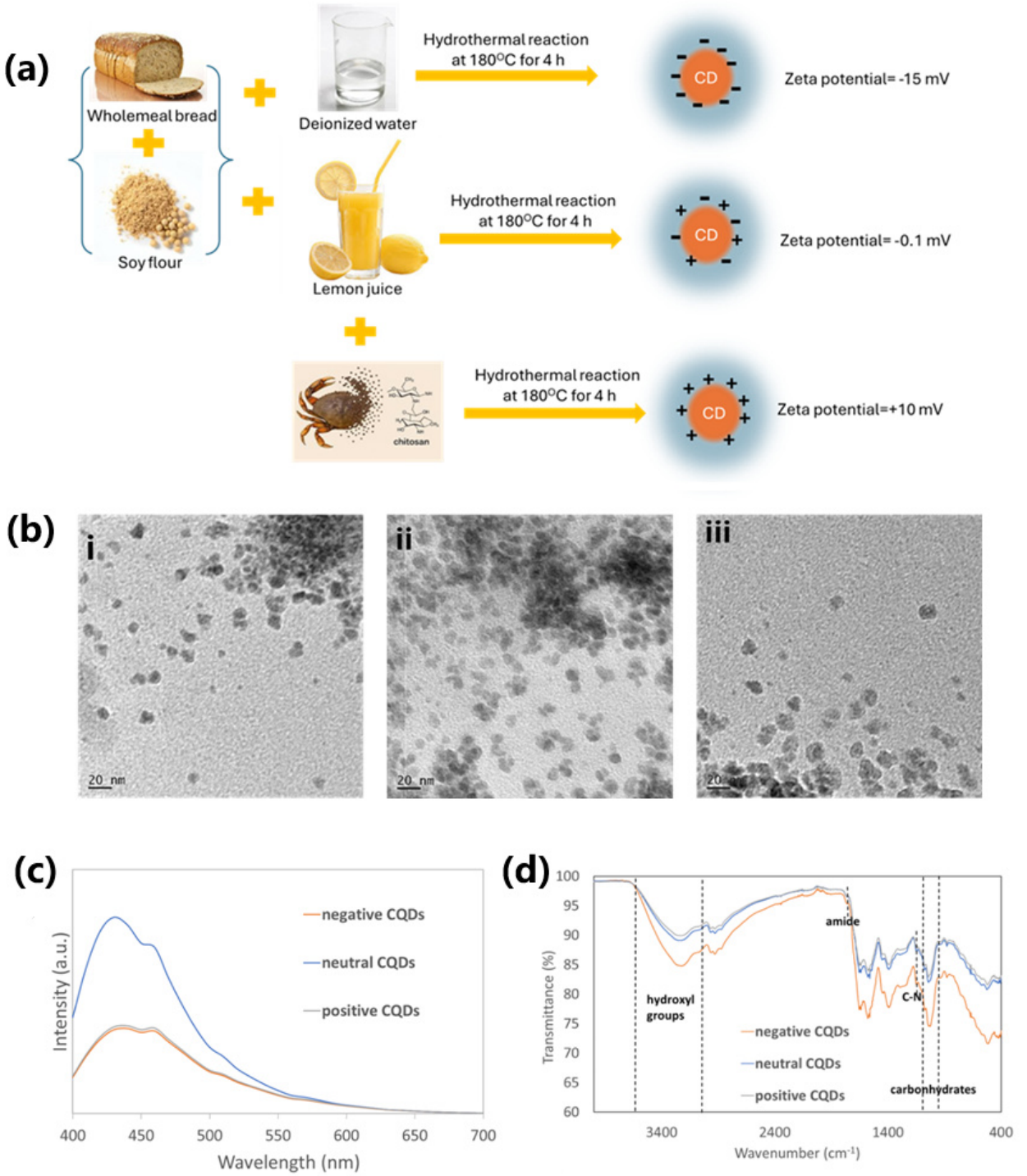

Figure 1. Characterizations of CQDs. (**a**) Precursors used in the synthesis and the measured surface charges; (**b**) TEM images of (i) negatively charged CQDs, (ii) neutrally charged CQDs, and (iii) positively charged CQDs; (**c**) fluorescence spectra; (**d**) FTIR spectra of three CQDs. CQDs: carbon quantum dots; FTIR: Fourier-transform infrared spectroscopy; TEM: transmission electron microscopy.

charged CQDs, suggesting that the carbohydrates were decomposed more significantly in the presence of lemon juice and chitosan. The broad band at 3,265 cm^{-1} was related to the stretching vibrations of the hydroxyl group. The strongest intensity of negatively charged CQDs corresponds to their high content of -OH and -COOH groups. The stretching vibration at 1,650 cm^{-1} was related to the amide group, and the peak at 1,150 cm^{-1} was attributed to the C-N bond, indicating that proteins were involved in the hydrothermal process.

The surface chemistry of the CQDs was analyzed by XPS. The survey spectra (Figure 2) indicated that all three CQDs mainly consisted of C, O, and N, indicating that N was successfully doped into the CQDs. The highest N content was found in positively charged CQDs (12.26 atomic percent [at.%] vs. 10.88 at.% for negative CQDs and 7.87 at.% for neutral CQDs) due to the addition of chitosan. According to a previous report, N doping substantially enhanced the optical properties of CQDs, and increasing the feeding amount of the N source gradually enhanced the quantum yield of the *N*-CQDs until a threshold was reached [34]. However, in this study, CQDs with the least N doping (neutral CQDs) had the highest fluorescence, suggesting that the photoluminescent properties of the CQDs are not solely dependent on the *N*-doping, but are more strongly influenced by surface charge.

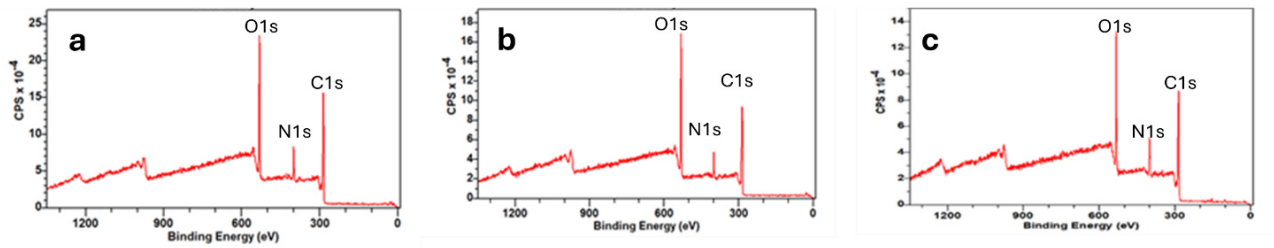

Figure 2. Survey XPS spectra of (a) negative CQDs, (b) neutral CQDs, and (c) positive CQDs. CQDs: carbon quantum dots; XPS: X-ray photoelectron spectroscopy.

The high-resolution C 1s spectra of the three CQDs are shown in Figure 3. The C peak was deconvoluted into three peaks at 288.32 eV, 286 eV, and 283.9 eV, attributed to C=O, C-O/C-N, and C-C bonds, respectively. Compared with negative CQDs, the C-O/C-N peak was less pronounced in neutral CQDs, indicating a lower density of oxygen- or nitrogen-containing surface groups, particularly hydroxyl, ether, or amine functionalities. When chitosan was introduced, the C-O/C-N peak intensity increased again, consistent with the incorporation of additional *N*-containing surface functional groups.

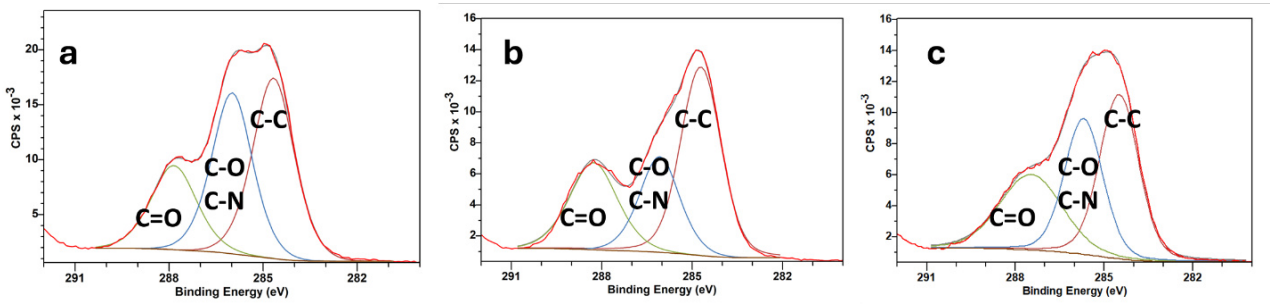

Figure 3. XPS C 1s spectra of (a) negative CQDs, (b) neutral CQDs, and (c) positive CQDs. CQDs: carbon quantum dots; XPS: X-ray photoelectron spectroscopy.

As shown in Figure 4, the O 1s spectra exhibited two peaks at around 531 eV and 533 eV, related to the C=O and C-O bonds, respectively. From Figure 4a to Figure 4c, the C=O peak gradually grew, and the ratio between C=O/C-O increased, suggesting an enrichment of carbonyl-containing functional groups on the CQD surface due to progressive surface oxidation. Previous studies have reported that strong oxidizing acids can carbonize small organic molecules into carbonaceous materials, which can subsequently be fragmented into smaller sheets through controlled oxidation [35]. In the present study, the presence of lemon juice in the preparation of neutrally and positively charged CQDs promoted the oxidative reaction of carbohydrates and achieved a more complete carbonization process. Notably, in the O 1s spectrum of positively charged CQDs, the C-O component is less than the C=O component, whereas in the C 1s spectrum the C-O/C-N component is significantly higher than the C=O component, suggesting increased contribution from C-N bonding, consistent with the introduction of nitrogen-rich functional groups from chitosan.

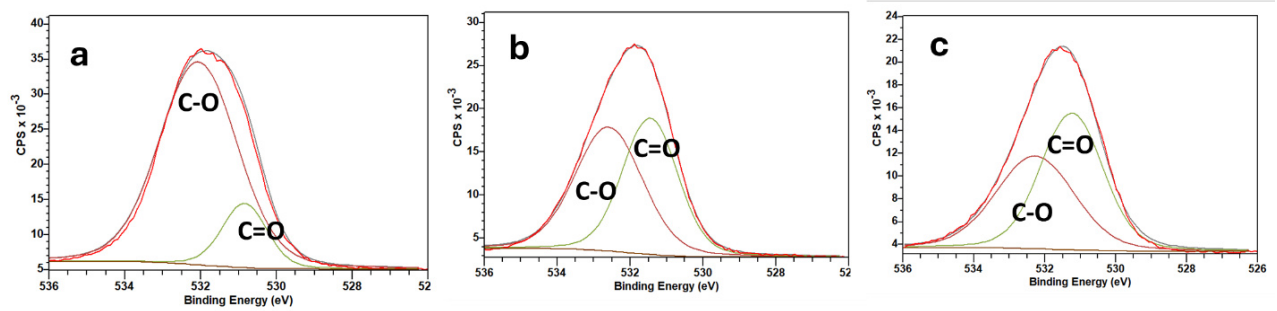

Figure 4. XPS O 1s spectra of (a) negative CQDs, (b) neutral CQDs, and (c) positive CQDs. CQDs: carbon quantum dots; XPS: X-ray photoelectron spectroscopy.

Figure 5 shows the N 1s spectra of the three CQDs. The peak at 399.5 eV is related to the pyrrolic or amine N, corresponding to N in five-membered rings or primary/secondary amine groups on the surface. A distinct peak above ~401 eV usually indicates protonated amines (-NH_3^+). The relative intensity of this peak increases from negatively to neutrally and positively charged CQDs, indicating increasing cationic (-NH_3^+) on the surface and an increasing abundance of surface cationic groups.

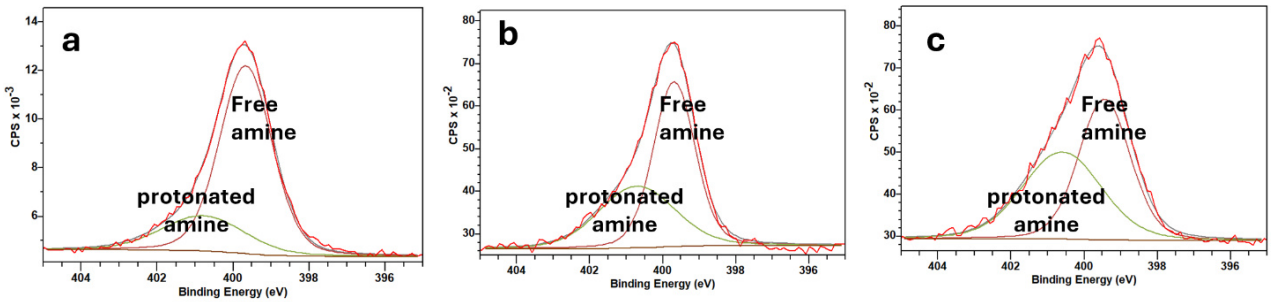

Figure 5. XPS N 1s spectra of (a) negative CQDs, (b) neutral CQDs, and (c) positive CQDs. CQDs: carbon quantum dots; XPS: X-ray photoelectron spectroscopy.

During the hydrothermal reactions of wholemeal bread and soy flour, their natural components decompose into carbonaceous fragments rich in oxygen-containing functional groups, mainly -COOH and -OH. In the presence of water, many of the -COOH groups become deprotonated to -COO^-, which imparts a net negative surface charge. Soy proteins and carbohydrates also undergo Maillard and dehydration reactions that further increase the formation of acidic oxygen-containing moieties. As a result, the CQDs produced from bread and soy flour are dominated by anionic functional groups, leading to a negative zeta potential. Lemon juice increases the cationic groups on CQDs because it contains high levels of citric acid (CA), which substantially lowers the pH of the reaction environment. In this acidic medium, the proteins and amino acids present in soybean flour undergo protonation, and their -NH_2 groups are converted into -NH_3^+, thereby introducing cationic sites on the CQD surface. The acidic conditions can also protonate -OH and C=O groups on intermediate carbonaceous fragments, which further increases the local positive charge density. In addition, CA provides COOH groups that, under low pH, remain protonated while the amine groups stay positively charged. As a result, the CQDs form surfaces that contain both cationic (-NH_3^+) and anionic (-COO^-) groups, ultimately giving rise to a zwitterionic structure with an overall neutral surface charge. Adding chitosan changes the neutral CQDs to positively charged CQDs because chitosan contains abundant amine groups that become protonated (-NH_3^+) under acidic hydrothermal conditions. During synthesis, these protonated amines are incorporated into the carbonaceous structure or adsorb onto the CQD surface, increasing the density of cationic functional groups. The number of positively charged -NH_3^+ groups contributed by chitosan exceeds the anionic groups present on the zwitterionic CQDs. As a result, the overall surface charge shifts from neutral to distinctly positive.

Overall, this study demonstrates a biogenic-precursor-driven strategy for precise surface-charge modulation of CQDs without the use of any synthetic reagents. By leveraging naturally occurring carbohydrates, proteins, organic acids, and biopolymers, the surface chemistry of CQDs can be systematically tuned from negative to zwitterionic and positive. This environmentally benign approach provides an effective means to tailor interfacial properties and offers a versatile platform for optimizing CQDs for various applications.

Biocompatibility

Owing to their biogenic origin, the CQDs are expected to exhibit good biocompatibility. This was further verified by evaluating the effects of CQDs with different surface charges on fibroblast cell proliferation. As shown in Figure 6, fibroblasts cultured in the presence of CQDs (1, 10, and 100 μg/ mL) exhibit proliferation behaviours comparable to those observed in the cell culture medium alone. No significant reduction in cell viability or growth rate was detected across all CQD variants, regardless of surface charge. These results indicate that the biogenic CQDs do not induce measurable cytotoxic effects toward fibroblast cells under the tested conditions. The comparable proliferation profiles suggest that surface charge modulation of CQDs does not adversely influence cell growth, highlighting their excellent biocompatibility and the potential for biomedical applications.

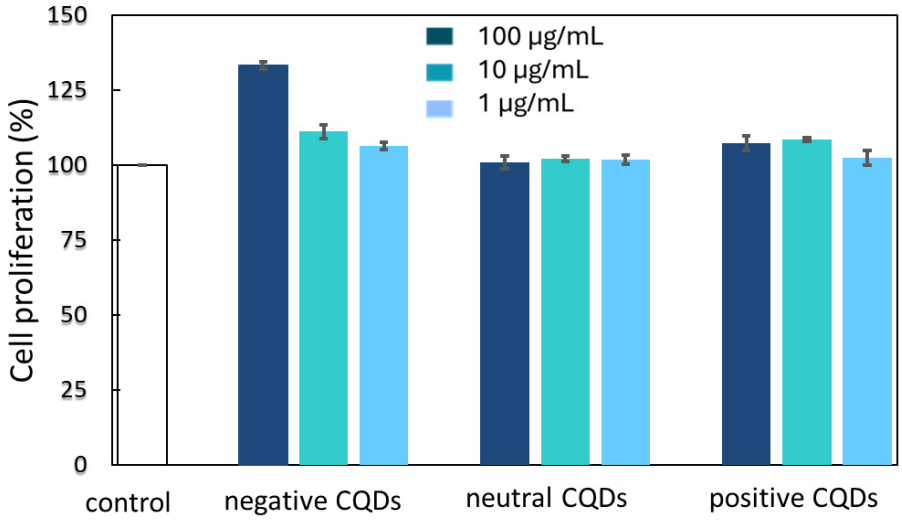

Figure 6. Biocompatibility in fibroblast cells for CQDs with various charges. CQDs: carbon quantum dots.

Interestingly, the negatively charged CQDs increased fibroblast proliferation to approximately 130% at 100 μg/mL, which was significantly higher than that of the untreated control ($p < 0.05$). Previous studies have shown that the surface charge of CQDs can strongly influence their cellular interactions and biological responses. Positively charged bovine serum albumin (BSA)-derived CQDs induced higher levels of inflammatory cytokine release in macrophages, whereas negatively charged CA-derived CQDs produced a comparatively lower inflammatory response [36]. This reduced inflammatory response may partly contribute to the enhanced fibroblast proliferation observed in the present study. However, Tang et al. [37] have also shown that the increased cell viability associated with CQDs may not be sustained during prolonged incubation, with the beneficial effect diminishing after 48–72 h. Therefore, the enhanced proliferation observed at 100 μg/mL in the present study may not necessarily indicate a sustained proliferative effect over longer exposure periods.

Antibacterial properties

The dominant organisms causing PJA infections are *Escherichia coli, Staphylococcus aureus*, and *Staphylococcus epidermidis*. These pathogens form biofilms on implant surfaces, making them highly

resistant to conventional antibiotics and host immune clearance. In orthopaedic implants, traditional antibiotic coatings and metallic nanoparticles (Ag and Cu) have shown limited long-term success due to cytotoxicity, antibiotic resistance, and loss of activity over time. Therefore, novel biocompatible nanomaterials with intrinsic antibacterial properties have been explored as alternatives to combat PJI in post-joint replacements.

Figure 7 presents the inhibition rates of CQDs at concentrations of 1, 10, and 100 μg/mL against *Escherichia coli*, *Staphylococcus aureus*, and *Staphylococcus epidermidis*. For *Escherichia coli*, the negatively charged CQDs exhibit only a weak antibacterial effect, whereas a pronounced increase in inhibition rate is observed for neutrally and positively charged CQDs. This behaviour can be attributed to the surface properties of *Escherichia coli*, whose outer membrane carries an overall negative charge due to the presence of lipopolysaccharides. The resulting electrostatic repulsion between the bacterial cell wall and negatively charged CQDs likely limits their interaction and cellular accessibility, thereby reducing antibacterial efficacy. In contrast, neutral and positively charged CQDs experience reduced electrostatic hindrance or electrostatic attraction, facilitating closer contact with the bacterial surface and enhancing antibacterial activity.

A similar charge-dependent trend is observed for *Staphylococcus aureus* and *Staphylococcus epidermidis.* As Gram-positive bacteria, they also possess an overall negative surface charge, which arises primarily from the abundance of negatively charged phosphate groups in teichoic acids (TAs) and lipoteichoic acids (LTAs) embedded within their thick peptidoglycan layer. This negatively charged cell envelope promotes electrostatic interactions with positively charged CQDs, thereby enhancing bacterial adhesion and antibacterial efficacy. Collectively, these observations confirm that surface charge is a key determinant governing CQD-bacteria interactions for both Gram-negative and Gram-positive strains.

With respect to concentration effects, the intermediate CQD concentration of 10 μg/mL produces the highest inhibition rates for all bacterial species. At lower concentrations (1 μg/mL), the number of CQDs is insufficient to induce effective bacterial inactivation. Conversely, the reduced antibacterial activity observed at 100 μg/mL may be attributed to the increased likelihood of CQD agglomeration at higher concentrations [38], which reduces the effective surface area available for interaction with bacterial cells and weakens their antibacterial performance. Overall, the results demonstrate that positively charged and neutrally charged CQDs at a concentration of 10 μg/mL exhibit the optimal antibacterial activity against *Escherichia coli*, *Staphylococcus aureus*, and *Staphylococcus epidermidis*, highlighting the importance of simultaneously optimizing surface charge and concentration to maximize antibacterial efficacy.

Discussion

Mechanisms underlying the biocompatibility and antibacterial properties of CQDs

Conventional antibacterial materials lack selectivity, indiscriminately killing bacteria while being cytotoxic to mammalian cells. There is an inherent trade-off between antibacterial potency and cytotoxicity, driven by shared mechanisms such as ROS production, membrane penetration, and intracellular interactions [39].

Interestingly, CQDs exhibit negligible cytotoxicity toward mammalian cells while demonstrating antibacterial activity against both Gram-negative and Gram-positive bacteria, especially for neutrally and positively charged CQDs. This selective behaviour primarily originates from fundamental structural and biochemical differences between bacterial and mammalian cells.

Bacterial cells are enclosed by rigid, highly charged cell walls composed of peptidoglycan. In Gram-negative bacteria, this structure is supplemented by an outer membrane rich in lipopolysaccharides, whereas Gram-positive bacteria are characterized by a thick peptidoglycan layer enriched with TA and LTA [40]. In both cases, these components impart a pronounced net negative surface charge, which promotes electrostatic attraction and close contact with charged nanoparticles such as CQDs. Neutrally and positively charged CQDs, in particular, interact strongly with negatively charged bacterial surfaces, enhancing nanoparticle adhesion, destabilizing the cell envelope, and ultimately inducing membrane permeabilization and leakage of intracellular constituents [41]. In contrast, mammalian cells lack a rigid cell wall and are

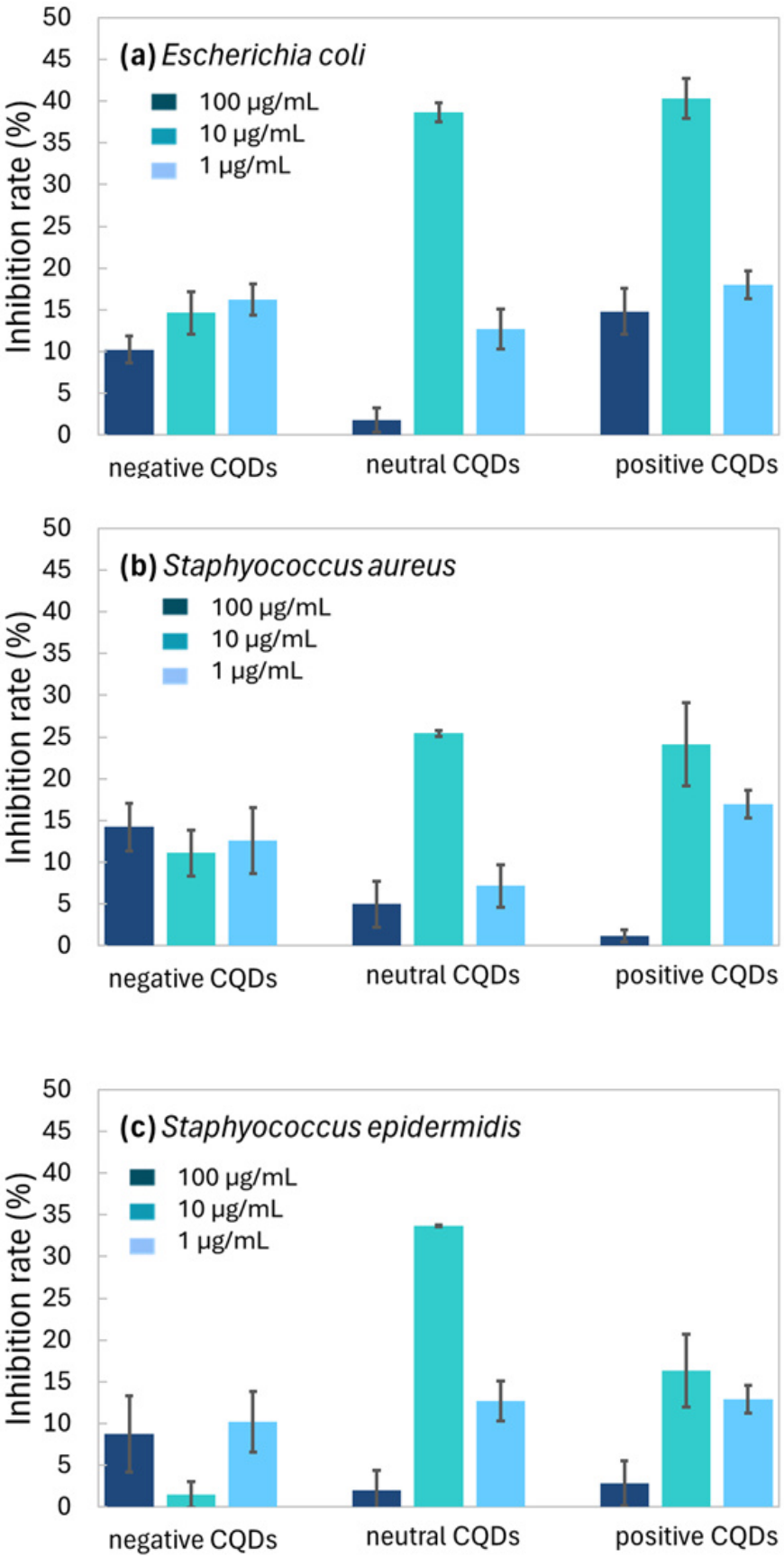

Figure 7. Inhibition rates of CQDs on (a) *Escherichia coli*, (b) *Staphylococcus aureus*, and (c) *Staphylococcus epidermidis*. CQDs: carbon quantum dots.

instead enclosed by a flexible lipid bilayer enriched with cholesterol and membrane-associated proteins. This structural organization confers greater mechanical stability and adaptability, effectively mitigating direct membrane disruption by CQDs. Consequently, the distinct surface charge characteristics and membrane architectures of bacterial and mammalian cells play a central role in enabling CQDs to selectively inhibit bacterial growth while maintaining high biocompatibility with mammalian cells.

Oxidative stress represents another important mechanism underlying the selective antibacterial activity of CQDs. These nanomaterials can generate ROS to cause severe oxidative damage to cellular components [42]. Bacterial cells generally exhibit limited antioxidant defence systems, rendering them highly sensitive to ROS-induced injury [43]. Mammalian cells, however, are equipped with more robust antioxidant mechanisms, including superoxide dismutase, catalase, and glutathione-based pathways [44], which effectively neutralize ROS at concentrations that are bactericidal but remain tolerable for host cells.

The differences in CQD internalization pathways further contribute to biocompatibility and antibacterial properties. Due to their ultrasmall size, CQDs can directly penetrate bacterial membranes, enabling intracellular interactions that disrupt essential biomolecules and metabolic processes [45]. In mammalian cells, uptake predominantly occurs via energy-dependent endocytosis, leading to sequestration of CQDs within endosomes or lysosomes [46]. This compartmentalization substantially attenuates cytotoxic effects unless CQDs are specifically engineered to escape these vesicular structures. Moreover, as prokaryotic organisms, bacteria lack intracellular compartmentalization [47], making critical components such as DNA, ribosomes, and enzymes immediately exposed once membrane integrity is compromised. In contrast, mammalian cells possess a high degree of compartmentalization, including membrane-bound organelles and a nuclear envelope, which provides additional layers of protection against nanoparticle-induced damage [48].

Collectively, these factors explain the intrinsic selectivity of CQDs, which enables efficient bacterial inactivation while minimizing cytotoxicity toward mammalian cells. This selective behaviour is particularly advantageous for biomedical and antimicrobial applications, which require potent antibacterial activity without adverse effects on normal tissues.

Potential applications of biogenic CQDs

Unlike conventional antibacterial agents that aim to eradicate bacteria, the neutrally and positively charged CQDs reported in this study can provide moderate antibacterial activity (inhibition rate 30–40%) while preserving 100% viability and function of mammalian cells. This combination of antibacterial activity and cytocompatibility may be beneficial in biomedical applications where bacterial suppression must be achieved while preserving host-cell function. For example, wound-dressing materials need to suppress bacterial growth while supporting the proliferation and function of skin cells during tissue repair. Materials that can suppress bacterial growth while maintaining mammalian cell viability may help reduce the risk of infection without compromising important cellular processes such as cell adhesion, proliferation, and differentiation. However, the suitability of moderate antibacterial activity will depend on the specific biomedical application and the severity of the infection.

Therefore, the development of CQDs with moderate antibacterial performance represents a strategic direction in biomaterials design. Such systems offer the potential to bridge the gap between antimicrobial protection and cytocompatibility, enabling safer and more effective applications in regenerative medicine and implantable technologies.

Conclusions

This study demonstrates that the surface charge of CQDs can be precisely tuned using biogenic materials through hydrothermal synthesis, entirely without chemical reagents, providing a fully green, environmentally friendly, and inherently biocompatible approach to producing functional CQDs. Wholemeal bread and soybean flour serve as the primary carbon sources and generate CQDs with negative surface charges (zeta potential ≈ –15 mV) because their decomposition products are rich in anionic

functional groups such as carboxyl and hydroxyl groups. Incorporating acidic lemon juice into the reaction medium alters the surface chemistry by introducing both protonated and deprotonated species, yielding CQDs with a zwitterionic surface (zeta potential ≈ –0.1 mV). This balance of cationic and anionic groups results in a net neutral charge. To produce positively charged CQDs, chitosan is added to the bread-soy-lemon precursor system. Chitosan contains amine groups that become protonated under acidic conditions, forming $-NH_3^+$. These protonated amines impart a positive surface charge to the resulting CQDs (zeta potential ≈ +10 mV). Both neutrally and positively charged CQDs at a concentration of 10 μg/mL show moderate antibacterial performance against both Gram-negative and Gram-positive bacteria, as their surfaces promote electrostatic interactions with the rigid, negatively charged bacterial cell envelopes, leading to membrane disruption, ROS-induced damage, and direct intracellular interference. Meanwhile, CQDs also exhibit excellent biocompatibility toward mammalian cells, as these cells are protected by flexible, cholesterol-rich membranes, robust antioxidant defences, and intracellular compartmentalization that together minimize CQD-induced cytotoxicity. The selectivity of CQDs enables efficient bacterial inactivation while maintaining minimal host cell toxicity, making them highly attractive for biomedical and antimicrobial applications for treating PJI.

Abbreviations

CA: citric acid

CQDs: carbon quantum dots

FTIR: Fourier-transform infrared spectroscopy

LTAs: lipoteichoic acids

PJI: periprosthetic joint infection

ROS: reactive oxygen species

TAs: teichoic acids

TEM: transmission electron microscopy

XPS: X-ray photoelectron spectroscopy

Declarations

Acknowledgments

The authors acknowledge the facilities and the scientific and technical assistance of the RMIT Microscopy & Microanalysis Facility (RMMF), a linked laboratory of Microscopy Australia.

Author contributions

HY: Conceptualization, Investigation, Supervision, Writing—original draft. MG: Investigation, Writing—review & editing. XG: Investigation, Writing—review & editing. TJS: Investigation, Writing—review & editing. PNS: Writing—review & editing. IC: Conceptualization, Supervision, Writing—review & editing. RWL: Conceptualization, Investigation, Supervision, Writing—review & editing. All authors read and approved the submitted version.

Conflicts of interest

The authors declare that they have no conflicts of interest.

Ethical approval

Not applicable.

Consent to participate

Not applicable.

Consent to publication

Not applicable.

Availability of data and materials

The datasets that support the findings of this study are available from the corresponding author upon reasonable request.

Funding

This research did not receive any specific grant from funding agencies in the public, commercial, or not-for-profit sectors.

Publisher's note

Open Exploration maintains a neutral stance on jurisdictional claims in published institutional affiliations and maps. All opinions expressed in this article are the personal views of the author(s) and do not represent the stance of the editorial team or the publisher.

References

1. Ozyurt D, Kobaisi MA, Hocking RK, Fox B. Properties, synthesis, and applications of carbon dots: A review. Carbon Trends. 2023;12:100276. [DOI]
2. Wang S, Wang D, Wang G, Zhang M, Sun Y, Ding J. Antibacterial carbon dots. Mater Today Bio. 2025; 30:101383. [DOI] [PubMed] [PMC]
3. Magalhães CM, Ribeiro E, Fernandes S, Esteves da Silva J, Vale N, Pinto da Silva L. Safety Evaluation of Carbon Dots in UM-UC-5 and A549 Cells for Biomedical Applications. Cancers. 2024;16:3332. [DOI] [PubMed] [PMC]
4. Li P, Sun L, Xue S, Qu D, An L, Wang X, et al. Recent advances of carbon dots as new antimicrobial agents. SmartMat. 2022;3:226–48. [DOI]
5. An Y, Wang Z, Wu FG. Fluorescent carbon dots for discriminating cell types: a review. Anal Bioanal Chem. 2024;416:3945–62. [DOI] [PubMed]
6. Zhao WB, Liu KK, Wang Y, Li FK, Guo R, Song SY, et al. Antibacterial Carbon Dots: Mechanisms, Design, and Applications. Adv Healthc Mater. 2023;12:e2300324. [DOI] [PubMed]
7. Lysenko V, Kuznietsova H, Dziubenko N, Byelinska I, Zaderko A, Lysenko T, et al. Application of Carbon Dots as Antibacterial Agents: A Mini Review. BioNanoScience. 2024;14:1819–31. [DOI]
8. Sun B, Wu F, Zhang Q, Chu X, Wang Z, Huang X, et al. Insight into the effect of particle size distribution differences on the antibacterial activity of carbon dots. J Colloid Interface Sci. 2021;584:505–19. [DOI] [PubMed]
9. Dong C, Wang Y, Chen T, Ren W, Gao C, Ma X, et al. Carbon Dots in the Pathological Microenvironment: ROS Producers or Scavengers? Adv Healthc Mater. 2024;13:e2402108. [DOI] [PubMed]
10. Amal NM, Shiddiq M, Armynah B, Tahir D. High reactive oxygen species produced from fluorescence carbon dots for anticancer and photodynamic therapies: A review. Luminescence. 2022;37:2006–17. [DOI] [PubMed]
11. Sun L, Zhao Y, Peng H, Zhou J, Zhang Q, Yan J, et al. Carbon dots as a novel photosensitizer for photodynamic therapy of cancer and bacterial infectious diseases: recent advances. J Nanobiotechnology. 2024;22:210. [DOI] [PubMed] [PMC]
12. Balou S, Shandilya P, Priye A. Carbon dots for photothermal applications. Front Chem. 2022;10: 1023602. [DOI] [PubMed] [PMC]

13. He L, Li Z, Gu M, Li Y, Yi C, Jiang M, et al. Intelligent Carbon Dots with Switchable Photo-Activated Oxidase-Mimicking Activity and pH Responsive Antioxidant Activity Adaptive to the Wound Microenvironment for Selective Antibacterial Therapy. Adv Sci. 2024;11:e2406681. [DOI] [PubMed] [PMC]
14. Liang J, Li W, Chen J, Huang X, Liu Y, Zhang X, et al. Antibacterial Activity and Synergetic Mechanism of Carbon Dots against Gram-Positive and -Negative Bacteria. ACS Appl Bio Mater. 2021;4:6937–45. [DOI] [PubMed]
15. Li RW, Alzaanin S, Yin Z, Smith PN. Quantum Osteoimmunology: A Paradigm Shift in Understanding and Influencing Bone-Immune Crosstalk. ChemMedChem. 2025;20:e202500307. [DOI] [PubMed] [PMC]
16. Hao X, Huang L, Zhao C, Chen S, Lin W, Lin Y, et al. Antibacterial activity of positively charged carbon quantum dots without detectable resistance for wound healing with mixed bacteria infection. Mater Sci Eng: C. 2021;123:111971. [DOI] [PubMed]
17. Zhao D, Zhang R, Liu X, Li X, Xu M, Huang X, et al. Screening of Chitosan Derivatives-Carbon Dots Based on Antibacterial Activity and Application in Anti-Staphylococcus aureus Biofilm. Int J Nanomed. 2022; 17:937–52. [DOI] [PubMed] [PMC]
18. Chen W, Yin H, Cole I, Houshyar S, Wang L. Carbon Dots Derived from Non-Biomass Waste: Methods, Applications, and Future Perspectives. Molecules. 2024;29:2441. [DOI] [PubMed] [PMC]
19. Gholipour A, Rahmani S. The Green Synthesis of Carbon Quantum Dots through One-step Hydrothermal Approach by Orange Juice for Rapid, and Accurate Detection of Dopamine. J Fluoresc. 2023;34:2665–77. [DOI] [PubMed]
20. Jin H, Gui R, Wang Y, Sun J. Carrot-derived carbon dots modified with polyethyleneimine and nile blue for ratiometric two-photon fluorescence turn-on sensing of sulfide anion in biological fluids. Talanta. 2017;169:141–8. [DOI] [PubMed]
21. Lai Z, Guo X, Cheng Z, Ruan G, Du F. Green Synthesis of Fluorescent Carbon Dots from Cherry Tomatoes for Highly Effective Detection of Trifluralin Herbicide in Soil Samples. ChemistrySelect. 2020;5:1956–60. [DOI]
22. Tyagi A, Tripathi KM, Singh N, Choudhary S, Gupta RK. Green synthesis of carbon quantum dots from lemon peel waste: applications in sensing and photocatalysis. RSC Adv. 2016;6:72423–32. [DOI]
23. Bandi R, Gangapuram BR, Dadigala R, Eslavath R, Singh SS, Guttena V. Facile and green synthesis of fluorescent carbon dots from onion waste and their potential applications as sensor and multicolour imaging agents. RSC Adv. 2016;6:28633–9. [DOI]
24. Boruah A, Saikia M, Das T, Goswamee RL, Saikia BK. Blue-emitting fluorescent carbon quantum dots from waste biomass sources and their application in fluoride ion detection in water. J Photochem Photobiol B: Biol. 2020;209:111940. [DOI] [PubMed]
25. Zhou J, Sheng Z, Han H, Zou M, Li C. Facile synthesis of fluorescent carbon dots using watermelon peel as a carbon source. Mater Lett. 2012;66:222–4. [DOI]
26. Atchudan R, Jebakumar Immanuel Edison TN, Shanmugam M, Perumal S, Somanathan T, Lee YR. Sustainable synthesis of carbon quantum dots from banana peel waste using hydrothermal process for in vivo bioimaging. Phys E: Low-dimens Syst Nanostructures. 2021;126:114417. [DOI]
27. Cui L, Ren X, Sun M, Liu H, Xia L. Carbon Dots: Synthesis, Properties and Applications. Nanomaterials. 2021;11:3419. [DOI] [PubMed] [PMC]
28. Gholipour A, Rahmani S. The synthesis of fluorescent carbon quantum dots for tartrazine detection in food: a novel one-step microwave heating approach. Fuller Nanotub Carbon Nanostructures. 2023;31: 743–51. [DOI]
29. Gokul Eswaran S, Thiruppathi D, Vasimalai N. Synthesis of highly fluorescent carbon dots from bread waste and their nanomolar lead ions sensor application. Environ Nanotechnol Monit Manag. 2022;18: 100748. [DOI]

30. Anpalagan K, Yin H, Cole I, Zhang T, Lai DTH. Quantum Yield Enhancement of Carbon Quantum Dots Using Chemical-Free Precursors for Sensing Cr (VI) Ions. Inorganics. 2024;12:96. [DOI]
31. Yin H, Chen W, Bratovic A, Li RW, Cole I. Carbon Quantum Dots as Emerging Antibacterial Nanomaterials: Strategies to Enhance Their Activity. C. 2026;12:46. [DOI]
32. K Anpalagan K, V Karakkat J, Truskewycz A, Saedi AA, Joseph P, Apostolopoulos V, et al. Bioimaging of C2C12 Muscle Myoblasts Using Fluorescent Carbon Quantum Dots Synthesized from Bread. Nanomaterials. 2020;10:1575. [DOI] [PubMed] [PMC]
33. Radchanka A, Hrybouskaya V, Iodchik A, Achtstein AW, Artemyev M. Zeta Potential-Based Control of CdSe/ZnS Quantum Dot Photoluminescence. J Phys Chem Lett. 2022;13:4912–7. [DOI] [PubMed]
34. Liao J, Cheng Z, Zhou L. Nitrogen-Doping Enhanced Fluorescent Carbon Dots: Green Synthesis and Their Applications for Bioimaging and Label-Free Detection of Au^{3+} Ions. ACS Sustain Chem Eng. 2016; 4:3053–61. [DOI]
35. Wang Y, Hu A. Carbon quantum dots: synthesis, properties and applications. J Mater Chem C. 2014;2: 6921. [DOI]
36. Usman M, Zaheer Y, Younis MR, Demirdogen RE, Hussain SZ, Sarwar Y, et al. The effect of surface charge on cellular uptake and inflammatory behavior of carbon dots. Colloid Interface Sci Commun. 2020;35:100243. [DOI]
37. Tang H, Lu C, Kodra O, Zhang J. Precursor effects on surface functionalization, photoluminescence, and cytotoxicity of carbon dots synthesized via microwave-assisted methods. Carbon Trends. 2025;21: 100579. [DOI]
38. Wu Y, Li C, van der Mei HC, Busscher HJ, Ren Y. Carbon Quantum Dots Derived from Different Carbon Sources for Antibacterial Applications. Antibiotics. 2021;10:623. [DOI] [PubMed] [PMC]
39. Makvandi P, Wang C, Zare EN, Borzacchiello A, Niu L, Tay FR. Metal-Based Nanomaterials in Biomedical Applications: Antimicrobial Activity and Cytotoxicity Aspects. Adv Funct Mater. 2020;30: e30. [DOI]
40. Doolan JA, Williams GT, Hilton KLF, Chaudhari R, Fossey JS, Goult BT, et al. Advancements in antimicrobial nanoscale materials and self-assembling systems. Chem Soc Rev. 2022;51:8696–755. [DOI] [PubMed] [PMC]
41. Cui T, Fan Y, Liu Y, Fan X, Sun Y, Cheng G, et al. Antibacterial Activity and Mechanism of Self-Assembly Spermidine-Capped Carbon Dots against Staphylococcus aureus. Foods. 2023;13:67. [DOI] [PubMed] [PMC]
42. Du X, Zhang M, Ma Y, Wang X, Liu Y, Huang H, et al. Size-dependent antibacterial of carbon dots by selective absorption and differential oxidative stress of bacteria. J Colloid Interface Sci. 2023;634: 44–53. [DOI] [PubMed]
43. Borisov VB, Siletsky SA, Nastasi MR, Forte E. ROS Defense Systems and Terminal Oxidases in Bacteria. Antioxidants. 2021;10:839. [DOI] [PubMed] [PMC]
44. Jomova K, Alomar SY, Alwasel SH, Nepovimova E, Kuca K, Valko M. Several lines of antioxidant defense against oxidative stress: antioxidant enzymes, nanomaterials with multiple enzyme-mimicking activities, and low-molecular-weight antioxidants. Arch Toxicol. 2024;98:1323–67. [DOI] [PubMed] [PMC]
45. Wang H, Song Z, Gu J, Li S, Wu Y, Han H. Nitrogen-Doped Carbon Quantum Dots for Preventing Biofilm Formation and Eradicating Drug-Resistant Bacteria Infection. ACS Biomater Sci Eng. 2019;5:4739–49. [DOI] [PubMed]
46. Yadav P, Shah K, Kansara K, Kumar A, Rawal R, Bhatia D. Tissue-Derived Primary Cell Type Dictates the Endocytic Uptake Route of Carbon Quantum Dots and *In Vivo* Uptake. ACS Appl Bio Mater. 2023;6: 1629–38. [DOI] [PubMed]
47. Surovtsev IV, Jacobs-Wagner C. Subcellular Organization: A Critical Feature of Bacterial Cell Replication. Cell. 2018;172:1271–93. [DOI] [PubMed] [PMC]

48. Havrdová M, Urbančič I, Bartoň Tománková K, Malina L, Štrancar J, Bourlinos AB. Self-Targeting of Carbon Dots into the Cell Nucleus: Diverse Mechanisms of Toxicity in NIH/3T3 and L929 Cells. Int J Mol Sci. 2021;22:5608. [DOI] [PubMed] [PMC]